Chemical sputtering of graphite by low temperature nitrogen plasmas at various substrate temperatures and ion flux densities

K. Bystrov,[1, a)] T. W. Morgan,[1] I. Tanyeli,[1] G. De Temmerman,[1] and M. C. M. van de Sanden[1]

FOM Institute DIFFER - Dutch Institute for Fundamental Energy Research, Association EURATOM-FOM, Partner in the Trilateral Euregio Cluster, P.O. Box 1207, NL-3430 BE Nieuwegein, The Netherlands

(Dated: 24 September 2013)

We report measurements of chemical sputtering yields of graphite exposed to low temperature nitrogen plasmas. The influence of surface temperature and incoming ion energy on the sputtering yields have been investigated in two distinct ion flux density regimes. Sputtering yields grow consistently with increasing temperatures in experiments with low flux density ($\Gamma_i \approx 10^{20}$ $m^{-2}s^{-1}$ – 10^{21} $m^{-2}s^{-1}$) and high flux density ($\Gamma_i \approx 10^{23}$ $m^{-2}s^{-1}$). Moreover, empirical fitting of the data suggests that the temperature of 670 ℃ is optimal for chemical sputtering at high flux density. Negative biasing of the samples was used to vary the ion energy in the low flux density regime. The sputtering yield in this case increases from 0.07 atoms/ion for E_i = 1.5 eV to 0.19 atoms/ion for E_i = 35 eV. After taking into account the dependence of the yields on temperature and ion energy we evidenced a flux dependence of sputtering, similar to that found for chemical sputtering of carbon by hydrogen.

[a)]Electronic mail: k.bystrov@differ.nl

I. INTRODUCTION

The theoretical prediction of outstanding mechanical properties of a hypothetical β-C_3N_4[1] compound resulted in a great interest in carbon nitride synthesis. There exists a wide variety of methods for preparation of carbon nitride films[2]. Many methods involve interactions of nitrogen ions with carbon surfaces[3]. Nitrogen is known to form chemical bonds with carbon atoms during ion bombardment[4], producing volatile molecules and chemically sputtering the surface. It was suggested that chemical sputtering was responsible for the observed limitations on nitrogen content and growth rates of the carbon nitride films[5]. Later, a number of research groups have detected CN and C_2N_2 molecules[6–13] with optical emission spectroscopy and mass spectrometry, confirming the importance of chemical sputtering for carbon nitride film growth.

In fusion research, hydrocarbon layers co-deposited in remote areas of tokamaks are very problematic because of their ability to retain intolerably large amounts of tritium[14]. Injection of nitrogen in the divertor area of a reactor is a proposed technique for reduction of the co-deposition[15]. The technique relies on the scavenging effect to reduce or completely supress film deposition. Scavenger particles are supposed to interact with reactive growth precursors in the gas phase, transforming them into non-reactive ones[16]. Decrease of hydrocarbon film growth rates in the presence of nitrogen-containing species in the plasma has been reported in laboratory experiments[17–20] as well as in tokamaks[21]. At the same time several authors[16,17,19] have stressed the importance of chemical sputtering during the scavenger experiments and showed that it must be taken into account when evaluating the effectiveness of such inhibition methods. Even if scavenging techniques based on nitrogen are not practical in tokamak environment, nitrogen is to be used to cool down the divertor plasma[22,23]. Consequently, the sputtering of the plasma-facing components due to nitrogen seeding in tokamaks also requires quantification[16,17,24]. Indeed, nitrogen capability of forming strong bonds with carbon and sputtering carbonaceous materials at a very high rate of about one atom per incoming ion[3,7,10,11,25,26] can be a potential lifetime concern for carbon-based plasma-facing components.

Despite the importance of chemical sputtering of carbon by nitrogen for various applications, little is known about the dependence of the sputtering yield on experimental parameters such as ion energy and surface temperature. In this context our paper addresses how

the sputtering yields behave with the varying ion energy and substrate temperature. We expand the existing database of the sputtering yields into the region of very low ion impact energies ($E_i \leq 35$ eV) and surface temperatures above $T_{surf} > 1000$ ℃. Moreover, we have performed experiments at varying plasma flux densities, ranging from $\Gamma_i \approx 4 \times 10^{20}$ $m^{-2}s^{-1}$ to $\Gamma_i \approx 4 \times 10^{23}$ $m^{-2}s^{-1}$.

II. EXPERIMENT

A. High flux density exposures in Pilot-PSI

Plasma exposures have been performed in two very different regimes in terms of the ion flux density. For simplicity we will call the two regimes "high flux" and "low flux". High flux experiments have been performed in the Pilot-PSI linear plasma generator. Detailed description of the experiment can be found elsewhere[27–30]. In brief, a cascaded arc plasma source[30,31] is used to produce the plasma, which exhausts into the vacuum vessel along the magnetic field axis. High electron density and temperature inside the source ($n_e = 10^{22}$ m^{-3}, $T_e = 1$ eV) create plasma with high dissociation and ionization degrees[32–34]. A strong axial magnetic field confines the plasma, generating an intense magnetized cylindrical plasma beam. Pilot-PSI operates in a pulsed mode. The pulse duration is limited by the cooling of the magnetic coils and is a function of the magnetic field strength. Throughout this work the field of 0.4 T was used. The maximum pulse duration in this case is 160 s. It takes approximately 1 s for the value of the magnetic field to reach its target value in the beginning of a pulse. The time of ramp down of the B-field at the end of the pulse is approximately 0.5 s. A water-cooled sample holder is located at a distance of 54 cm from the exhaust of the plasma source and is installed perpendicularly to the magnetic field.

Typical line-integrated optical emission spectrum of the nitrogen plasma near the sample is shown in Figure 1. There are no molecular nitrogen bands visible in the spectrum. This allows us to conclude that N^+ is the dominant ion in the Pilot-PSI beam. Plasma electron density and electron temperature were measured by Thomson scattering[35] at a distance of ∼25 mm upstream from the plasma facing surface. The typical profiles of electron density n_e, electron temperature T_e and ion flux density Γ_{N^+} are shown in Figure 2. The flux density is calculated assuming that the ions are accelerated up to the sound velocity and that the

plasma density in the sheath drops by a factor of two compared to the pre-sheath values. Typical full width at half maximum (FWHM) of the nitrogen plasma beam is ∼20 mm. The flux density profile is then integrated over the surface of the sample to obtain the average ion flux to the surface as well as the total fluence.

A fast infrared (IR) camera (SC7500-MB, FLIR) was employed to monitor the surface temperature of the samples during exposure. The waveband of the camera spans from 1.5 μm to 5.1 μm. 2D surface temperature profiles were measured with a spatial resolution of 0.3 mm. Additionally, a multiwavelength pyrometer (FMPI SpectroPyrometer, FAR associates) is used to determine the surface emissivity. The pyrometer integrates the emission spectrum from 0.87 μm to 1.65 μm and for the graphite samples can measure temperatures above 300 ℃. An emissivity value of 0.7 provided a good agreement between the two measurements.

B. Low flux density exposures in nano-PSI

A different set-up − nano-PSI − was used to expose graphite surfaces to nitrogen plasma at lower flux densities (10^{20} $m^{-2}s^{-1}$ − 10^{21} $m^{-2}s^{-1}$). It has a spherical vacuum vessel and 20 observation ports aimed at the center. A combination of a roots pump and a turbo-molecular pump provides a base pressure of about 10^{-7} mbar. The plasma is generated by a cascaded arc source of the same type as in Pilot-PSI. However, the plasma in nano-PSI is not magnetized. The sample holder is positioned in the center of the vacuum vessel, approximately 30 cm away from the nozzle of the plasma source. Samples can be either heated or water-cooled. The temperature of the samples is monitored via a K-type thermocouple that can be inserted into the sample or spot-welded to it. A single wavelength pyrometer (Dr. Georg Mauer GmbH, TMR-95d) is used to cross-check the temperature of the sample during the exposures. The samples can be either electrically floating or biased.

The following procedure is used to create nitrogen plasmas is nano-PSI. The source generates an arc in argon with a discharge current of 40 − 90 A. Nitrogen is injected into the expanding argon plasma through a ring surrounding the plasma and situated at a distance of several centimeters from the nozzle of the source (Figure 3). The ring is electrically floating. The typical argon throughput of the source is 3.0 slm, while the nitrogen injection rate is 0.3 slm (standard liter per minute; 1 slm = 4.4×10^{20} particles/s). Argon-nitrogen plasmas have been studied in detail in a similar setup by Brussaard[34,36] and de Graaf[37,38].

They have developed a plasma chemistry model, where the following reactions between the species influence the plasma composition:

$$Ar^+ + N_2 \rightarrow Ar + N_2^+ \quad (1)$$

$$N^+ + N_2^* \rightarrow N + N_2^+ \quad (2)$$

$$N_2^+ + e \rightarrow N^* + N \quad (3)$$

In brief, molecular nitrogen ions are produced in charge exchange reactions between Ar^+ and N^+ and neutral background and are lost via recombination with electrons. The ratio of the species, electron density and electron temperature depend on the distance from the plasma source, as well as the input power of the plasma source and the ratio between argon and injected nitrogen. The model reproduced Langmuir probe measurements of the exponential drop in electron density from 10^{19} m^{-3} at the location of the nitrogen injection to 10^{18} m^{-3} at the distance of 30 cm downstream (the location of the sample in our experiment). Electron temperature at the same location was found to be around 0.6 eV for the case of nitrogen to argon gas ratio of 10%. These measurements by de Graaf suggest an ion flux of the order of 10^{21} $m^{-2}s^{-1}$ at the location of the sample, which is consistent with our measurements of the ion saturation current to negatively biased samples. The particle fluxes to the surface are more than two orders of magnitude smaller compared to Pilot-PSI, since the radial diffusion towards the walls of the vacuum chamber is not prevented by the magnetic field and is an important particle loss mechanism. The plasma is broad enough to neglect spatial variations of the flux density across the surface of the sample and consider the plasma profile flat. The experimental conditions in Pilot-PSI and nano-PSI are summarized in Table I.

We have used optical emission spectroscopy to determine the optimal nitrogen-to-argon ratio, in order to maximize the N_2^+ concentration at the location of the sample. The spectra recorded for four different seeding ratios are presented in Figure 4. Reference case without nitrogen injection shows a number of prominent argon lines (Figure 4a). The emission is due to the decay of highly excited Ar^{**} atoms, produced in the three particle recombination reaction[38]:

TABLE I. Summary of experimental conditions during nitrogen plasma experiments in Pilot-PSI and nano-PSI

	Pilot-PSI	nano-PSI
Arc current used (A)	150 − 200	40 − 90
Nitrogen throughput (slm)	1.5 − 2.0	0.3 (+ 3.0 slm Ar)
Base pressure (mbar)	2×10^{-3}	$10^{-6} - 10^{-7}$
Magnetic field (T)	0.4 (up to 1.6 T available)	no field
Pulse duration (s)	160 (at 0.4 T)	steady state
Ion species	N^+	N_2^+
Flux density ($m^{-2}s^{-1}$)	$2 \times 10^{23} - 2 \times 10^{23}$	$4 \times 10^{20} - 2 \times 10^{21}$
Electron temperature (eV)	0.7 − 1.0	0.5 − 0.6
Sample temperature (℃)	200 − 1000	100 − 800

$$Ar^+ + e + e \rightarrow Ar^{**} + e \tag{4}$$

As 5% of nitrogen is injected into the plasma molecular nitrogen bands become visible on the optical emission spectrum. Namely, the N_2 $C^3\Pi_u - B^3\Pi_g$ Second Positive System (SPS) and the N_2^+ $B^2\Sigma_u^+ - X^2\Sigma_g^+$ First Negative System (FNS) can be recognized immediately (Figure 4b). Notably, argon line emission is still dominant in the spectrum of the 95% Ar - 5% N_2 plasma. Increase of the injected amount of nitrogen to 10% results in supression of argon lines and dominance of the N_2^+ FNS in the 360 nm − 430 nm range (Figure 4c). Further increase of the nitrogen seeding amount results in decrease of the integral emission from the plasma (Figure 4d).

The relative emission intensities from different species are visualized in Figure 5 for the same four cases with different nitrogen seedings. For this purpose the N_2 SPS bandhead at 380.5 nm, the N_2^+ FNS bandhead at 391.4 nm and the Ar I line at 415.9 nm are compared. The respective bands and the argon line are color-coded in Figure 4 for convenience. The Ar I line actually overlaps with the N_2^+ FNS ($\Delta\nu = -1$) band, which spans from 411.0 nm to 427.8 nm, so the intensity of argon emission is likely overestimated for the cases with 10% and 17% of nitrogen injetion. Since the N_2^+ FNS emission is maximal for the 10% of nitrogen

seeding scenario, it was selected for performing the graphite sputtering experiments. These measurements are in agreement with the findings of Brussaard[36], who has determined the ion to electron mass ratio in such plasmas numerically using the plasma chemistry model. At a distance of 15 cm from the nozzle he has has calculated $m_+/m_e \approx 5\times10^4$. This corresponds to Z $\approx$ 27 for the plasma ions. Such Z value suggests that already at 15 cm from the nozzle the number of agron ions in the plasma is negligible, and the plasma consists predominantly of N_2^+ ions.

C. Sample preparation and characterization

The samples used in this study were machined out of fine-grain graphite (R6650, SGL-Carbon). The samples for Pilot-PSI are 4 mm thick disks with a diameter of 30 mm, while 20×20×4 mm square samples were used in nano-PSI. Prior to exposure all samples were mechanically polished and ultrasonically cleaned using acetone and then alcohol. In Pilot-PSI the samples were clamped onto a water cooled copper heat sink. We used flexible grafoil® sheet as an interface between graphite and copper to improve the thermal contact between the two. The clamping ring was shielding a small part of the sample periphery from plasma impact, so the effective exposed diameter of the sample in this mounting configuration was in fact 26 mm. In nano-PSI the samples were held in position by three stainless steel screws, thus minimizing the area shielded from the plasma.

The sputtering yield for each exposed sample is calculated using post-mortem mass loss measurements. The typical mass loss for the exposed samples is in the milligram range. Such considerable mass loss is not only significantly larger than the sensitivity of the balance (Mettler-Toledo MS105DU, standard deviation 0.08 mg), but also allows us to neglect the contributions from absorbed water or retained gas. In addition, it has been checked that sample handling during mounting and dismounting cannot introduce a noticeable systematic error in the sputtering yield calculations. Insertion of a thermocouple also has no noticable affect on the mass of the sample. Furthermore, sample heating in vacuum, but without plasma exposure does not lead to a detectable mass loss. Mass loss in milligrams is converted into the number of carbon atoms lost from the surface, which is then divided by the measured ion flux to obtain the sputtering yield.

To supplement the post-mortem mass loss measurements we have attempted to detect the

products of the chemical reaction with a residual gas analyzer (RGA) and optical emission spectroscopy (OES). Both methods were not sensitive enough to accomplish this task. Due to a large gas throughput of the cascaded arc plasma sources the mass spectra measured by the RGA in both machines were dominated by the signal corresponding to the working gas, while the signals from CN, C_2N_2 and HCN were on the noise level. Additional problem with using the RGA on Pilot-PSI is the requirement to locate it several meters away from the magnetic field coils in order to avoid noise pick up from strong currents in the coils. As for the OES measurements, we couldn't detect the CN $B^2\Sigma - X^2\Sigma$ violet system (bandhead around 388 nm). In nano-PSI the band was probably obscured by the N_2^+-FNS emission. In Pilot-PSI measurements with a band pass filter could allow longer integration times without saturating the signal at other wavelenghts.

Scanning electron microscopy (SEM) was used to image these modifications for the exposed samples. Selected samples from Pilot-PSI have been analyzed using surface profilometer to visualize the sputtering pattern cerated by the plasma beam.

III. RESULTS

Throughout the article we draw parallels between chemical sputtering by nitrogen and chemical sputtering by hydrogen. Sputtering by these reactive species is similar in terms of processes that lead to carbon atoms leaving the surface, namely, the rearrangement of bonds in carbon lattice, formation of new chemical bonds and molecules, their diffusion to the surface, desorption or sputtering. Contrary to chemical sputtering by nitrogen, sputtering by hydrogen has been studied for decades, extensively quantified and described by established models. That is why we find that references to hydrogen are sometimes necessary to facilitate interpretation of the measurements of sputtering by nitrogen.

A. Substrate temperature dependencies of the sputtering yields

Decades of research dedicated to chemical sputtering by hydrogen demontrated that the chemical sputtering yield is a complex function of ion energy, surface temperature and ion flux[39]. Until demonstated otherwise, it is reasonable to assume that sputtering yields by nitrogen also depend on these parameters.

First, we establish how surface temperature variation influences the sputtering yield in Pilot-PSI and nano-PSI. In case of hydrogen-carbon interaction the occurence of an 'optimal' temperature for chemical sputtering is believed to originate from the competition of an exponential increase of the reaction rate between carbon and hydrogen with an even stronger decrease of the hydrogen concentration in the surface at elevated temperatures[40]. The existence of a similar effect for nitrogen is yet to be demonstrated. Only a few dedicated experiments studying the temperature dependence have been performed to date[10,11,26], and the results are not complete and sometimes even contradictory. Specifically, Schlüter[26] and colleagues found no changes of the sputtering yield for temperatures ranging from -163 ℃ to 67 ℃. Morrison[11] observed a decrease of the sputtering yield for temperatures increasing from room temperature to around 430℃, while Grigull[10] reported an opposite trend for temperatures in the 200 ℃ $-$ 800 ℃ range. In parallel, it was observed that an increase of surface temperature leads to lower deposition rates of carbon nitride films[41–43], decreased nitrogen concentration in the films[44–49] and increased surface roughness[50], all indirectly suggesting the existence of a noticeable surface temperature dependence of the chemical sputtering by nitrogen.

Sputtering yields for samples exposed in Pilot-PSI are plotted against the temperature in Figure 6. Same plasma source settings were used for all exposures. The sputtering increases by about an order of magnitude when the temperature is increased from around 200 ℃ up to 400 ℃. For samples exposed at temperatures above 800 ℃ sputtering yields decrease with temperature. The reason for the lack of data in the 400℃ $-$ 800 ℃ range is the following. In Pilot-PSI the heating of the sample surface occurs because of the high heat flux from the plasma. Surface temperatures can be varied by changing the torque applied to the screws that clamp the sample to the sample stage, since the quality of the thermal contact depends on the pressure applied to the grafoil® sheet[51]. Of course, this is a very crude approach that provides variation, but not a real way of controlling the surface temperature. Fitting suggests a maximum yield at 670℃. Note, that at this time we use a purely empitical fit that is not representing a model for chemical sputtering as a function of temperature.

Independent temperature control was possible in nano-PSI using resistive sample heating. We have observed an increasing trend for the sputtering yield with temperature, which is consistent with results from Pilot-PSI. Specifically, the yield increased by a factor of about two when the temperature was changed from 150℃ to 650 ℃ (see Figure 7). The maximum

achievable temperature of 650℃ makes it impossible to detect a maximum in the sputtering yield.

B. Sputtering yields at various energies

For some time only estimations of the sputtering yield of carbon by nitrogen were available[7,10,25]. In those experiments N_2^+ ions with energies exceeding the physical sputtering threshold of carbon have been used. Thus, the estimated sputtering yields describes the combination of physical and chemical sputtering. First measurements of the energy dependence of the sputtering yield were reported by Morisson *et al.*,[11] and Jacob *et al*[3]. Both groups have used N_2^+ ion beams and carbon films in their studies. Jacob *et al.* managed to quantify sputtering at energies as low as 30 eV per N_2^+ ion. They have provided clear evidence that sputtering at these low energies is a chemical process. Further experiments and analysis[26] led to a model describing sputtering of carbon films by nitrogen at low energies. To expand the existing database of the sputtering yields we performed low energy exposures, quantifying sputtering at energies below 30 eV for the first time.

Sputtering yield measurements for samples from Pilot-PSI have been performed only for floating samples, since biasing in nitrogen leads to sputtering of the molybdenum clamping ring and contamination of the surface with trace amounts of molybdenum. In floating configuration the energy of the nitrogen ions is determined by acceleration in the sheath and is not sufficient to sputter molybdenum. Ions, accelerated in the sheath, arrive at the surface with an energy of approximately $5kT_e$, that is 5 eV for the case of $T_e = 1$ eV, assuming that electron and ion temperatures in the plasma are equal. In nano-PSI we have used the biasing voltages of -10 V, -20 V, -30 V and -70 V to vary the energy of impinging ions. To have a direct comparison between sputtering by molecular ions in nano-PSI and atomic ions in Pilot-PSI as well as to compare our results with the existing data it was assumed that N_2^+ ions behave like two N^+ ions at half energy. This allows normalization of the energy and the yield to the effective atomic flux.

Results of the measurements on Pilot-PSI and nano-PSI are plotted in Figure 8. The datapoints from both experiments are corrected for the surface temperature dependence. Datapoints recorded at the same energy are averaged and the scatter of the data points is included in the error bars. Previously published data[3,7,10,11,25,26] are added for comparison.

Data points from other experiments are not corrected for temperature differences, since the temperature dependence in those experiments might be different from what we have observed. Sputtering yields in Pilot-PSI are of the order of 5×10^{-3} atoms/ion, which is significantly lower than in any other experiment. Sputtering yields from nano-PSI are an order of magnitude higher than in Pilot-PSI at the same ion energy. Sputtering yields increase with the ion energy and seem to saturate at the level of 0.17 atoms/ion. Sputtering yields measured by Jacob, Morrison and others are generally of the order of $0.5 - 1.0$ atoms/ion (normalized to the effective atomic flux), even higher than in nano-PSI. This difference might be caused by the choice of the sample material, as will be discussed later.

It is worth commenting on the behaviour of the sputtering yield at very low energies in nano-PSI. The datapoint corresponding to electrically floating samples, for which the ion energy was the lowest, stands out from the trend somewhat. Here, the sputtering yield is the same (within the error bar) as that for the sample biased at -10 V. At first, this might seem surprising. However, removal of carbon from a floating graphite surface might be driven by chemical erosion, instead of a combination of chemical erosion and chemical sputtering. Chemical erosion does not require energetic species since it is a thermally activated process[52], while chemical sputtering starts to play a role when the kinetic energy of the projectiles is sufficient to influence the yield. And indeed, for the floating samples the energy of the impinging nitrogen ions was around 3 eV. Since the binding energy of carbon atoms in graphite is 7 eV, the ions should start breaking additional carbon bonds, creating sites for chemical reactions with incoming nitrogen, only when the sample is negatively biased.

IV. DISCUSSION

A. Sputtering at different flux densities

A possible explanation of the observed difference in sputtering between the low flux and the high flux regimes is the dependence of the sputtering yield on the ion flux. Such dependence has for a long time been a point of debate in the case of sputtering by hydrogen. One of the first models of sputtering due to methane formation[53] decribes the influence of the ion flux density on the temperature dependence of the chemical yield[54]. An analytical model[39] built later using data from many experiments with fluxes up to $\Gamma_i \leq 6 \times 10^{23}$ m^{-2}s^{-1}

established the dependence of the chemical erosion yield on the ion flux to $\Phi^{-0.54}$. It was suggested that the hydrogenation of the carbon surface is the rate-limiting process that hinders the sputtering yields at high fluxes. Already at the flux density of 10^{23} $m^{-2}s^{-1}$ a carbon atom would on average experience ten impacts with impinging hydrogen ions during the 1 ms[55] that is needed for a hydrocarbon molecule to form and leave the surface[56]. The rate-limiting role of the surface hydrogenation is consistent with the inverse dependence of the sputtering yield on the flux density.

The sputtering by nitrogen should follow the same general steps as sputtering by hydrogen, namely, rearrangement of chemical bonds in the process of formation of volatile components weakly bonded to the surface and their subsequent removal from the surface. Thus, one could speculate that in this case nitrogenation of the surface would be a rate-limiting mechanism decreasing the sputtering yield as flux increases and eventually leading to saturation of the amount of sputtered atoms. We have measured the sputtering yields in the broad range of flux densities, spanning from 4×10^{20} $m^{-2}s^{-1}$ to 4×10^{23} $m^{-2}s^{-1}$. The results are consistent with the existence of a rate-limiting mechanism. Indeed, as Figure 9 demonstrates, the sputtering yield is more than an order of magnitude lower for high flux density exposures. Note, that the data in this figure is corrected to account for temperature and ion energy variations in different exposures. If we were to fit the data in the similar way as Roth did for hydroden, we would have obtained a very similar expression for the flux dependence, namely $\Phi^{-0.48\pm0.03}$. Of course, this result is very preliminary, since it relies on two data sets only and assumes the flux dependence assumes the form of Φ^{-x}.

Let us now describe how sensitive are these results to the redeposition of sputtered carbon, presence of neutrals in the plasma and surface roughening due to plasma treatment of surfaces.

B. Role of redeposition

The problem of quantifying sputtering can be complicated by redeposition. Atoms and molecules redeposited on the same surface from which they were initially eroded can not be accounted for with mass loss measurements. This can lead to an underestimation of the gross sputtering yield. Earlier experiments in Pilot-PSI[57] have demonstrated that in hydrogen up to 90% of sputtered carbon atoms are redeposited locally, resulting in a difference of one

order of magnitude between the gross and net sputtering yields. Presence of redeposition in that case was easily observed with surface profilometry and SEM.

Results of profilometry and SEM observations for samples exposed to nitrogen suggest that redeposition is much weaker than for hydrogen. The typical result of surface profiling for a graphite sample exposed to nitrogen in Pilot-PSI is given in Figure 10. The reference level is chosen using the edges of the sample that were shielded from the plasma by the clamping ring. Contrary to what was observed for hydrogen[56,57] under similar experimental conditions in terms of density, temperature and surface temperature, the profile is concave and does not exhibit regions of prominent redeposition. The profile has roughly the same shape as the incoming ion flux density profile in Figure 2.

Surface morphology changes due to exposure to nitrogen plasma also point towards lesser role redeposition plays during nitrogen exposures. Figure 11a shows that nitrogen plasma irradiation in Pilot-PSI creates a pronounced pattern of sharp cone- or pyramid-like structures on the entire graphite surface. This particular image was taken after 300 seconds of plasma irradiation, so the roughening of the surface happens relatively quickly. In general, such morphology can be considered characteristic for chemically sputtered graphite surfaces as it has been observed in various sputtering experiments[58,59]. It has also been observed in hydrogen experiments on Pilot-PSI[57], but only in the *erosion-dominated areas* on the periphery of the samples. Strong redeposition promoted growth of carbon particles in the central regions of the sample. On the contrary, in nitrogen the pattern with sharp structures is charactristic for the entire surface.

At relatively low plasma densities in nano-PSI redeposition should not play a significant role by default, since the plasma is transparent for the neutrals leaving the surface. Interestingly enough, samples exposed to low flux density plasmas exhibit similar morphology, only in this case the size of the structures is much smaller (see Figure 11b). This is not surprising, since not only the flux density, but also the fluence in nano-PSI is much smaller than in Pilot-PSI. Consequently, we are likely observing the initial stages of the surface roughening. Similarities in surface morphology between different experiments and even formed by different species imply that formation of such structures is a generic result of chemical sputtering, rather than an experiment-specific effect. Hansen[60] proposed an explanation of the surface roughness evolution in sputtering experiments. In brief, initial roughness creates an imbalance of flux between the hills and the valleys. Enhanced flux to hilltops leads to

local thermal spikes and promotes graphitization. As a consequence, there also exists an imbalance in local sputtering yields (which depend on surface temperature) between the hills and valleys and surface roughness changes with time.

C. Effect of surface roughening

Calculation of the sputtering yield requires knowledge of the exact ion flux collected by the exposed surface. In our calculations we treat the exposed surfaces as flat. However, plasma-induced surface roughening increases the effective area that collects the ions and thus introduces an uncertainty in the calculation. Exact calculation of the effective surface area is not feasible, however we can try to estimate the uncertainty. If we approximate the structures on the surface as square pyramids, the plasma-collecting area of each structure would be equal to $l\sqrt{l^2 + (2h)^2}$, where h is the height of the pyramid and l is the length of the base. From the SEM images (Figure 11) we could say that h and l are approximately equal. This would mean that we may overestimate the flux densities (thus underestimating the yields) by a factor of $\sqrt{5}$.

D. Presence of neutrals

Neutral nitrogen atoms and molecules can induce chemical etching of graphite via the following reactions[38]:

$$\mathrm{C}(solid) + \mathrm{N} \rightarrow \mathrm{CN}(gas) \tag{5}$$

$$2\mathrm{C}(solid) + \mathrm{N_2} \rightarrow 2\mathrm{CN}(gas) \tag{6}$$

Reaction 5 is weakly exothermic (0.17 eV for N(^{4}S), while reaction 6 is strongly endothermic (4.7 eV at 298 K)[61]. If neutrals take part in the sputtering of graphite in our experiments, they would be unaccounted for in the flux calculations and, consequently, the sputtering yields would be overestimated. It therefore important to comment on their role in sputtering in both experimental setups.

1. Neutrals in Pilot-PSI

The spectrum in Figure 1 is dominated by N I lines meaning that atomic nitrogen is produced in Pilot-PSI. Yet, we believe that there is not enough neutral particles in the central region of the plasma beam to make a significant contribution to the measured sputtering yields.

As a first order approximation we estimate the pressure of ions in the plasma beam and compare it with the measured pressure in the vessel during the plasma exposure. The ion pressure in the beam with n_e=10^{20}m^{-3} and $T_i = T_e = 1$ eV is about 15 Pa. This is about five times larger than the measured vessel pressure. Furthermore, the radial profile of the density of neutrals is hollow. Indeed, nitrogen atoms are produced in charge-exchange reactions between nitrogen ions and the background gas and via dissociative recombination of molecular ions (equations 2 and 3, respectively). It is necessary to estimate the penetration depth of the background nitrogen molecules into plasma beam. The cross section for charge-exchange between atomic ions and molecular nitrogen (Equation 2) can be estimated as 5×10^{20}m^{-3}[62]. Using the plasma density of 10^{20}m^{-3}, $T_i = T_e = 1$ eV, and T_{gas} = 100 ℃, we obtain 1 mm for the mean free path for charge-exchange. This is ten times smaller than the typical radius of the nitrogen plasma beam. The rate for dissociative recombination of molecular ions (Equation 3) is three orders of magnitude larger than the rate for charge exchange[36,63], making the lifetime of molecular ions very short and confining them to the narrow region on the periphery of the plasma beam. From this we conclude that the nitrogen atoms are produced mainly on the periphery of the plasma beam, where most of the light emission originates. The situation is similar to that in hydrogen plasma, where the neutral density profile decreases sharply towards the center of the beam and the emission profile is hollow as was explained in detail by Shumack[64]. Taking this into account we conclude that the ionic flux to the surface issignificantly larger than the atomic flux in Pilot-PSI and the sputtering of carbon is caused predominantly by nitrogen ions.

2. Neutrals in nano-PSI

Studies of argon/nitrogen expanding plasmas[34,38] demonstrated presence of energetic neutral nitrogen species in the plasma, such as metastable N_2 ($A^3\Sigma_u^+$) molecules. Brussard

showed that the structure of the N_2^+-FNS band, namely overpopulation of the vibrational levels 6 and 7, is consistent with a charge exchange reaction between atomic ions in the ground state and the metastable molecules in the N_2 ($A^3\Sigma_u^+$) state[34]. The radiative lifetime of the N_2 ($A^3\Sigma_u^+$) molecule is longer than the residence time of gas in the vessel and it can enter the plasma with an energy of around 6 eV[38]. Brussaard has calculated the density of the metastables for different electron densities[34]. For densities in the $10^{18}m^{-3}$ range, typical for nano-PSI plasmas used in this study, he obtained a value of around $10^{19}m^{-3}$ for the concentration of the N_2 ($A^3\Sigma_u^+$). However, only 10% of the metastables succeed in returing to the center of the plasma due to collisional quenching of the metastable state[34]. The Abel inverted intensity of the N_2^+-FNS band allowed to draw a conclusion that most of the neutrals stay in the periphery of the plasma[38]. Taking into account these results, it is possible to estimate that the density of metastables near the sputtered surface is of the same order as the density of the ions. To quantify the effect on the measured sputtering yields we have exposed a positively biased sample in nano-PSI. Bias of 7.5 V was selected to repel positive ions and to collect only electrons and neutrals on the surface. In principle, some of the ions from the tail of the Maxwellian distribution could have reached the surface, but higher biasing was not possible due to overheating of the sample holder by the electron current. The measured mass loss then corresponds to erosion of carbon by nitrogen neutrals at a given temperature. The experiment was performed at 600 ℃, which is a favorable temperature for chemical sputtering in nano-PSI. The detected mass loss was about four times smaller compared to exposures with negative bias. We conclude that the neutrals can be responsible of up to 25% of the carbon sputtering in nano-PSI. The uncertainty associated with the energetic ions reaching the positively biased surfaces makes this an upper estimate of erosion by neutrals.

E. Effect of the type of material

The samples for our experiments were machined out of fine-grain graphite, while other research groups have used amorphous hydrocarbon films. So far there is no direct experimental comparison of the sputtering yields of graphite and amorphous films. At the same time, first experiments with diamond (boron-doped CVD diamond produced at Element Six Ltd.[65]) in nano-PSI resulted in sputtering yields about 1.5 times lower than for graphite

under the same loading conditions. It is possible to argue that the difference in binding energies of carbon atoms in graphite and films should cause a variation in sputtering yields. Studies of chemical sputtering by hydrogen indeed demonstrate larger sputtering yields for amorphous films[52,66–68] and smaller yields for diamond films[69,70] in comparison with graphite. The dependence of the yield on the structural properties is particularly high for low energies of projectiles[52], so in the regime where we have performed experiments. Additionaly, the presence of hydrogen in amorphous films could influence the rate at which carbon is removed from the surface. Indeed, volatile HCN[3] is one of the possible products of the chemical reactions happening at the surface. Since the ratio at which HCN and other volatile componds (CN and/or C_2N_2) are formed is unknown, it is impossible to say how significant is the effect of the hydrogen presence. Different types of materials used might be one of the reasons for the sputtering yields from nano-PSI to be generally lower in comparison with the experiments with carbon films.

V. CONCLUSIONS

Graphite samples have been exposed to low temperature nitrogen plasmas in order to quantify sputtering of carbon. The measurements were aimed at expanding the existing database of the sputtering yields of carbon by nitrogen. The sputtering is chemical by nature, since the kinetic energy of the impinging ions in these experiments was below the physical sputtering threshold. Experiments have been performed in two distinct regimes in terms of plasma density and ion flux. The low flux regime was established in nano-PSI with ion flux densities of the order of 10^{21} $m^{-2}s^{-1}$, while the high flux regime was achieved in Pilot-PSI linear plasma generator and characterized by flux densities of the order of 10^{23} $m^{-2}s^{-1}$. Variation of substrate temperature in both experiments influenced the sputtering yields in a consistent manner. Increase of temperature from 150 ℃ to about 700 ℃ in nano-PSI resulted in a steady increase of the sputtering yield. Similar trend is observed in Pilot-PSI, however it is reversed when the temperature exceeds 800 ℃. Thus, in Pilot-PSI the temperature of 670 ℃ is optimal for sputtering. Empirical fitting of the data allows to correct the datapoints recorded at different energies for differences in temperature. Experiments with different biasing voltages in nano-PSI show that the sputtering yields increase with impinging ion energy and seem to saturate at the level of 0.17 atoms/ion.

This is lower than in the previously published reports about sputtering of carbon films with nitrogen ion beams, probably due to the different type of the substrate used. Values obtained for the yields in the high flux scenario are an order of magnitude lower than in the low flux bombardment with the same energy. Redeposition of 90% of carbon would have explained the difference, but judging from profilometry results and SEM images it is much less pronounced. Presence of energetic neutrals in nano-PSI also can not explain a difference of one order of magnitude between the yield measured at different fluxes. From this we conclude that the likely exists a flux dependence of the sputtering yield, similarly to that observed for sputtering by hydrogen. Further experiments at various fluxes, as well as better quantification of redeposition, surface roughening and neutral background would lead to a better quantification of this dependence. Moreover, experiments with hydrogen-nitrogen plasma mixtures are necessary to extrapolate the present results to tokamak experiments. It is, for example, unknown, how the surface temeperature and flux dependence of the sputtering yield would behave in the presence of nitrogen.

It is not surprising that the sputtering yield of carbon by nitrogen is a complex function of surface temperature, ion energy and ion flux density. Our experiments contribute the understanding of these dependencies by increasing the range of parameters for which the sputtering has been quantified.

ACKNOWLEDGMENTS

The authors would like to thank Richard Al, Marc van de Pol, Hennie van der Meiden, Peter Wortman and the Pilot-PSI team for their support in preparation and execution of the experiments. We would also like to thank Laurent Marot and Daniel Mathys from University of Basel for helping with the SEM images, as well as Andrey Litnovsky and Maria Matveeva from Forschungszentrum Jülich for helping with profilometry measurements. This work was supported by the European Communities under the Contract of Association between EURATOM/FOM and carried out within the framework of the European Fusion Programme with financial support from NWO and the NWO Grant RFBR 047.018.002. The views and opinions expressed herein do not necessarily reflect those of the European Commission.

REFERENCES

[1]A. M. Liu and M. L. Cohen, Phys. Rev. B 41(15), 10727 (1990).

[2]S. Muhl and J. M. Méndez, Diamond Relat. Mater. 8, 1809 (1999).

[3]W. Jacob, C. Hopf, and M. Schlüter, Appl. Phys. Lett. 86, 204103 (2005).

[4]J. A. Taylor, G. M. Lancaster, and J. W. Rabalais, J. Am. Chem. Soc. 100 (14), 4441 (1978).

[5]S. S. Todorov, D. Marton, K. J. Boyd, A. H. Al-Bayati, and J. W. Rabalais, J. Vac. Sci. Technol. A 12 (6), 3192 (1994).

[6]N. V. Novikov, M. A. Voronkin, A. A. Smekhnov, N. I. Zaika, and A. P. Zakharchuk, Diam. Relat. Mater. 4, 390 (1995).

[7]P. Hammer and W. Gissler, Diam. Relat. Mater. 5, 1152 (1996).

[8]R. Kaltofen, T. Sebald, and G. Weise, Thin Solid Films 290-291, 112 (1996).

[9]J. Hong and G. Turban, Diamond Relat. Mater. 8, 572 (1999).

[10]S. Grigull, R. Behrisch, and S. Parascandola, J. Nucl. Mater. 275, 158 (1999).

[11]N. A. Morisson, S. E. Rodil, J. Robertson, and W. I. Milne, J. Appl. Phys. 89 (10), 5754 (2001).

[12]N. Hellgren, M.P. Johansson, E. Broitman, P. Sandström, L. Hultman, and J.-E. Sundgren, Thin Solid Films 382, 146 (2001).

[13]Z. W. Deng and R. Souda, Surf. Sci. 488, 393 (2001).

[14]J. Roth, E. Tsitrone, T. Loarer, V. Philipps, S. Brezinsek, A. Loarte, G. F. Counsell, R. P. Doerner, K. Schmid, O. V. Ogorodnikova, and R. A. Causey, Plasma Phys. Control. Fusion 50, 103001 (2008).

[15]F. L. Tabarés, D. Tafalla, I. Tanarro, V. J. Herrero, A. Islyaikin, and C. Maffiotte, Plasma Phys. Control. Fusion 44, L37 (2002).

[16]T. Schwarz-Selinger, C. Hopf, C. Sun, and W. Jacob, J. Nucl. Mater. 363-365, 174 (2007).

[17]W. Bohmeyer, F. L. Tabarés, M. Baudach, A. Cwiklinski, A. Markin, T. Schwarz-Selinger, J.A. Ferreira, G. Fussmann, and A. Loarte, J. Nucl. Mater. 390-391, 560 (2009).

[18]F. L. Tabarés, J. A. Ferreira, A. Ramos, G. van Rooij, J. Westerhout, R. Al, J. Rapp, A. Drenik, and M. Mozetic, Phys. Rev. Lett. 105, 175006 (2010).

[19]E. Vassallo, S. Barison, A. Cremona, G. Grosso, M. Fabrizio, and L. Laguardia, Plasma Phys. Control. Fusion 52, 075014 (2010).

[20]E. Vassallo, A. Cremona, L. Laguardia, and G. Grosso, Plasma Phys. Control. Fusion 53, 032002 (2011).

[21]F. L. Tabarés, D. Tafalla, V. Rohde, M. Stamp, G. Matthews, G. Esser, V. Philipps, R. Doerner, and M. Baldwin, J. Nucl. Mater. 337-339, 867 (2005).

[22]L. C. Ingesson, J. Rapp, and G. F. Matthews, J. Nucl. Mater. 313-316, 1173 (2003).

[23]A. Kallenbach, M. Bernert, T. Eich, J.C. Fuchs, L. Giannone, A. Herrmann, J. Schweinzer, W. Treutterer, and the ASDEX Upgrade Team, Nucl. Fusion. 52 (12), 122003 (2012).

[24]S. Brezinsek, S. Jachmich, J. Rapp, A. G. Meigs, C. Nicholas, M. O'Mullane, A. Pospieszczyk, G. van Rooij, and JET-EFDA contributors, J. Nucl. Mater. 417, 624 (2011).

[25]P. Sundelin, C. Schulz, V. Phillips, M. Rubel, G. Sergienko, and L. Marot, J. Nucl. Mater. 390-391, 647 (2009).

[26]M. Schlüter, C. Hopf, and W. Jacob, New J. Phys. 10, 053037 (2008).

[27]V. P. Veremiyenko, Ph.D. thesis, An ITER-relevant magnetized hydrogen plasma jet. (Eindhoven, The Netherlands, 2006).

[28]J. Westerhout, W. R. Koppers, W. A. J. Vijvers, R. S. Al, S. Brezinsek, S. Brons, H. J. N. van Eck, R. Engeln, B. de Groot, R. Koch, H. J. van der Meiden, M. P. Nuijten, V. Philipps, M. J. van de Pol, P. R. Prins, U. Samm, J. Scholten, D. C. Schram, B. Schweer, P. H. M. Smeets, D. G. Whyte, E. Zoethout, A. W. Kleyn, W. J. Goedheer, N. J. Lopes Cardozo and G. J. van Rooij, Phys. Scr. T128, 18 (2007).

[29]G. J. van Rooij, V. P. Veremiyenko, W. J. Goedheer, B. de Groot, A. W. Kleyn, P. H. M. Smeets, T. W. Versloot, D. G. Whyte, R. Engeln, D. C. Schram, and N. J. Lopes Cardozo, Appl. Phys. Lett. 90(12), 121501 (2007).

[30]W. A. J. Vijvers, C. A. J. van Gils, W. J. Goedheer, H. J. van der Meiden, D. C. Schram, V. P. Veremiyenko, J. Westerhout, N. J. Lopes Cardozo, and G. J. van Rooij, Phys. Plasmas 15(9), 093507 (2008).

[31]G. M. W. Kroesen, D. C. Schram, and J. C. M. de Haas, Plasma Chem. Plasma P. 10, 531 (1990).

[32]M. C. M. van de Sanden, G. M. Janssen, J. M. de Regt, D. C. Schram, J. A. M. van der Mullen, and B. van der Sijde Rev. Sci. Instrum. 63, 3369 (1992).

[33]M. C. M. van de Sanden, J. M. de Regt, and D. C. Schram, Plasma Sources Sci. Technol. 3, 501 (1994).

[34]G. J. H. Brussaard, Ph.D. thesis, Remote Arc Generated Plasma in Diatomic Gases (Eind-

hoven, The Netherlands, 1999).

[35]H. J. van der Meiden, R. S. Al, C. J. Barth, A. J. H. Donné, R. Engeln, W. J. Goedheer, B. de Groot, A. W. Kleyn, W. R. Koppers, N. J. Lopes Cardozo, M. J. van de Pol, P. R. Prins, D. C. Schram, A. E. Shumack, P. H. M. Smeets, W. A. J. Vijvers, J. Westerhout, G. M. Wright, and G. J. van Rooij, Rev. Sci. Instrum. 79(1), 013505 (2008).

[36]G. J. H. Brussaard, M. C. M. van de Sanden, and D. C. Schram, Phys. Plasmas 4(8), 3077 (1997).

[37]A. de Graaf, G. Dinescu, J. L. Longueville, M. C. M. van de Sanden, D. C. Schram, E. H. A. Dekempeneer, and L. J. van Ijzendoorn, Thin Solid Films 333, 29 (1998).

[38]A. de Graaf, Ph.D. thesis, Deposition of CNH Materials: Plasma and Film Characterization. (Eindhoven, The Netherlands, 2000).

[39]J. Roth, A. Kirschner, W. Bohmeyer, S. Brezinsek, A. Cambe, E. Casarotto, R. Doerner, E. Gauthier, G. Federici, S. Higashijima, J. Hogan, A. Kallenbach, H. Kubo, J.M. Layet, T. Nakano, V. Philipps, A. Pospieszczyk, R. Preuss, R. Pugno, R. Ruggieri, B. Schweer, G. Sergienko, and M. Stamp, J. Nucl. Mater. 337-339, 970 (2005).

[40]W. Jacob and J. Roth, Chemical Sputtering. In: R. Behrisch, W. Eckstein, editors. Sputtering by Particle Bombardment (Springer, Berlin Heidelberg New York, 2007), pp. 329-400.

[41]W. T. Zheng, H. Sjöstrom, I. Ivanov, K. Z. Xing, E. Broitman, W. R. Salaneck, J. E. Greene, and J.-E. Sundgren, J. Vac. Sci. Technol. A 14 (5), 2696 (1996).

[42]G.-Q. Yu, S.-H. Lee, D.-G. Lee, H.-D. Na, H.-S. Park, and J.-J. Lee, Surf. Coat. Tech. 154, 68 (2002).

[43]J. M. Stillahn and E. R. Fisher, J. Phys. Chem. C 113, 1963 (2009).

[44]H. Sjöstrom, I. Ivanov, M. Johansson, L. Hultman, J.-E. Sundgren, S. V. Hainsworth, T.F. Page, and L.R. Wallenberg, Thin Solid Films 246, 103 (1994).

[45]Yang B.-C., N. Tajima, T. Sogoh, O. Takai, Chen Z.-H., Chin. Phys. Lett. 16 (11), 847 (1999).

[46]Z. Y. Chen, J. P. Zhao, T. Yano, T. Ooie, M. Yoneda, and J. Sakakibara, J. Appl. Phys. 88 (12), 7060 (2000).

[47]Z. W. Deng and R. Souda, Thin Solid Films 406, 46 (2002).

[48]J. Neidhardt, H. Högberg, and L. Hultman, Surf. Sci. 569, L289 (2004).

[49]C. Spaeth, U. Kreissig, and F. Richter, Thin Solid Films 355-356, 64 (1999).

[50]Y. H. Cheng, X. L. Qiao, J. G. Chen, Y. P. Wu, C. S. Xie, Y. Q. Wang, D. S. Xu, S. B. Mo, and Y. B. Sun, Diam. Relat. Mater. 11, 1511 (2002).

[51]M. A. van den Berg, S. Brons, O. G. Kruijt, J. Scholten, R. Pasquet, P. H. M. Smeets, B. Schweer, and G. De Temmerman, Fus. Eng. Design 86, 1745 (2011).

[52]W. Jacob and J. Roth, Chemical Sputtering. In: R. Behrisch, W. Eckstein, editors. Sputtering by Particle Bombardment (Springer, Berlin Heidelberg New York, 2007), pp. 329-400.

[53]S. K. Erents, C. M. Braganza, and G. M. McCracken, J. Nucl. Mater. 63, 399 (1976).

[54]J. Roth and C. García-Rosales, Nucl. Fusion 36 (12), 1647 (1996).

[55]J. Roth, J. Nucl. Mater. 266-269, 51 (1999).

[56]G. J. van Rooij, J. Westerhout, S. Brezinsek, and J. Rapp, J. Nucl. Mater. 415, S137 (2011).

[57]K. Bystrov, L. van der Vegt, G. De Temmerman, C. Arnas, and L. Marot, J. Vac. Sci. Technol. A. 31 (1), 011303 (2013).

[58]R. Pugno, M. J. Baldwin, R. P. Doerner, J. Hanna, D. Nishijima, and G. Antar, J. Nucl. Mater. 363, 1277 (2007).

[59]H. Zhang, F. W. Meyer, H. M. Meyer III, and M. J. Lance, Vacuum 82(11), 1285 (2008).

[60]T. A. R. Hansen, J. W. Weber, P. G. J. Colsters, D. M. H. G. Mestrom, M. C. M. van de Sanden, and R. Engeln, J. Appl. Phys. 112, 013302 (2012).

[61]S. Veprek, J. Crystal Growth, 17, 101 (1972).

[62]R. F. Stebbings, B. R. Turner, and A. C. H. Smith, J. Chem. Phys., 38, 2277 (1963).

[63]J. B. Hasted, Physics of Atomic Collisions, 2nd ed., (Butterworths, London 1972).

[64]A. E. Shumack, et al., Phys. Rev. E, 78, 046405 (2008).

[65]G. De Temmerman, et al., Nucl. Fusion, 51, 052001 (2011).

[66]E. Vietzke, K. Flaskamp, V. Philipps, G. Esser, P. Wienhold, and J. Winter, J. Nucl. Mater. 145-147, 443 (1987).

[67]D. L. Youchison, M. D. Nahemow, R. T. McGrath, and A. J. Baratta, J. Nucl. Mater. 176-177, 461 (1990).

[68]K. Katayama, H. Nagase, C. Nishinakamura, T. Takeishi, and M. Nishikawa, Fus. Eng. Design 81A (1-4), 247 (2006).

[69]C. M. Donnelly, R.W. McCullough, and J. Geddes, Diam. Relat. Mater. 6, 787 (1997).

[70]G. De Temmerman, R. P. Doerner, P. John, S. Lisgo, A. Litnovsky, L. Marot, S. Porro, P.

Petersson, M. Rubel, D. L. Rudakov, G. Van Rooij, J. Westerhout, and J. I. B. Wilson, Phys. Scr. T138, 014013 (2009).

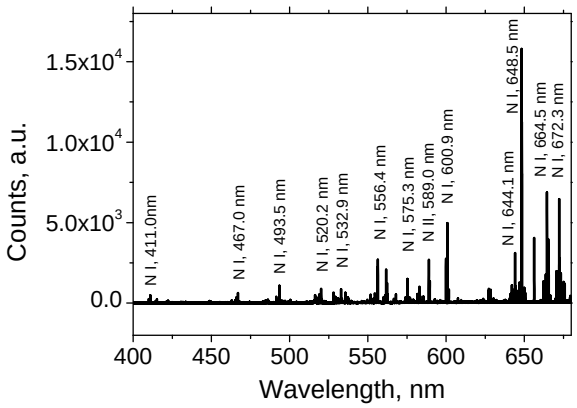

FIG. 1. Typical optical emission spectrum from nitrogen plasma in Pilot-PSI. The spectrometer was positioned to have a tangential view on the plasma near the location of the sample. The spectrum is line inegrated.

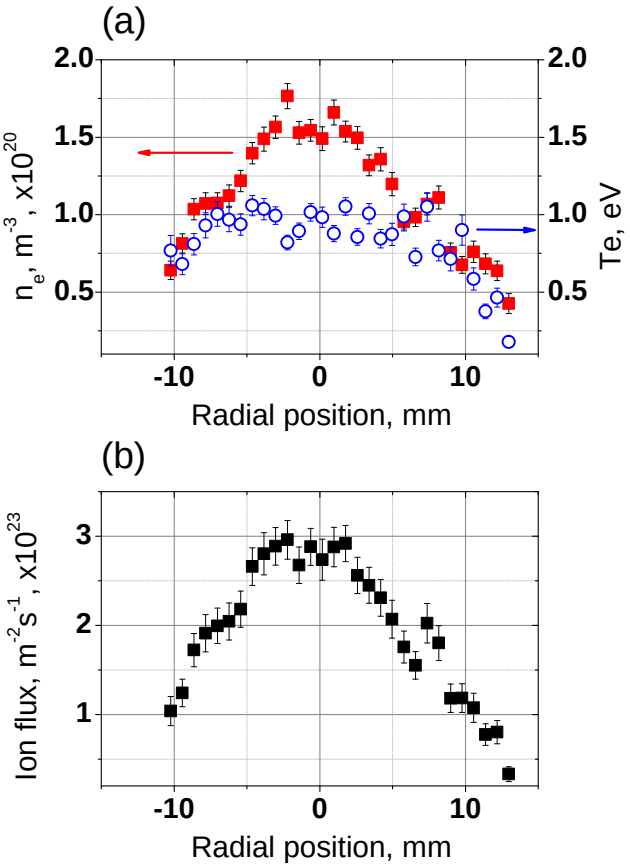

FIG. 2. Typical radial profiles of electron density, temperature (a) and ion flux density (b) of the nitrogen plasma beam in Pilot-PSI obtained from Thomson scattering.

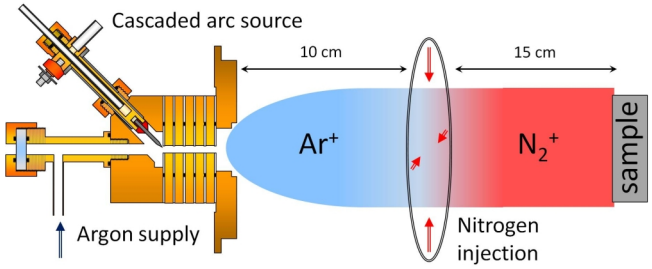

FIG. 3. Schematic of the experiment in nano-PSI. The cascaded arc source created pure argon plasma into which nitrogen is injected. The flux of nitrogen ions is produced by recombination and impinges the sample surface. The incoming flux is derived from the ion saturation current on the sample.

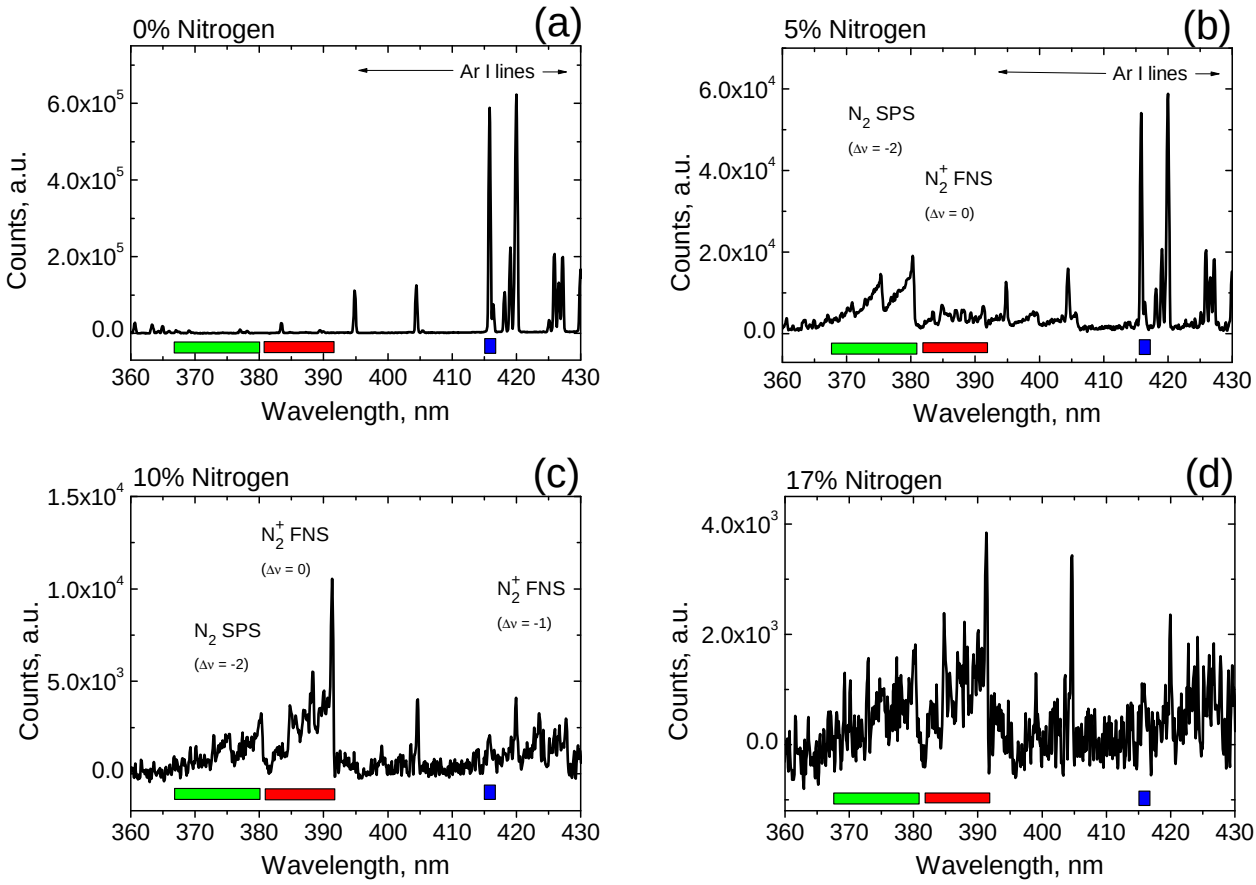

FIG. 4. Optical emission spectra of argon plasmas with different admixtures of nitrogen - 0% (a), 5% (b), 10% (c) and 17% (d). Molecular nitrogen bands are clearly visible when the fraction of injected nitrogen is 5% (b) and dominate the spectrum when this fraction is 10% (c). Further increase of the injected nitrogen amount leads to decrease of the integral emission from the plasma (d)

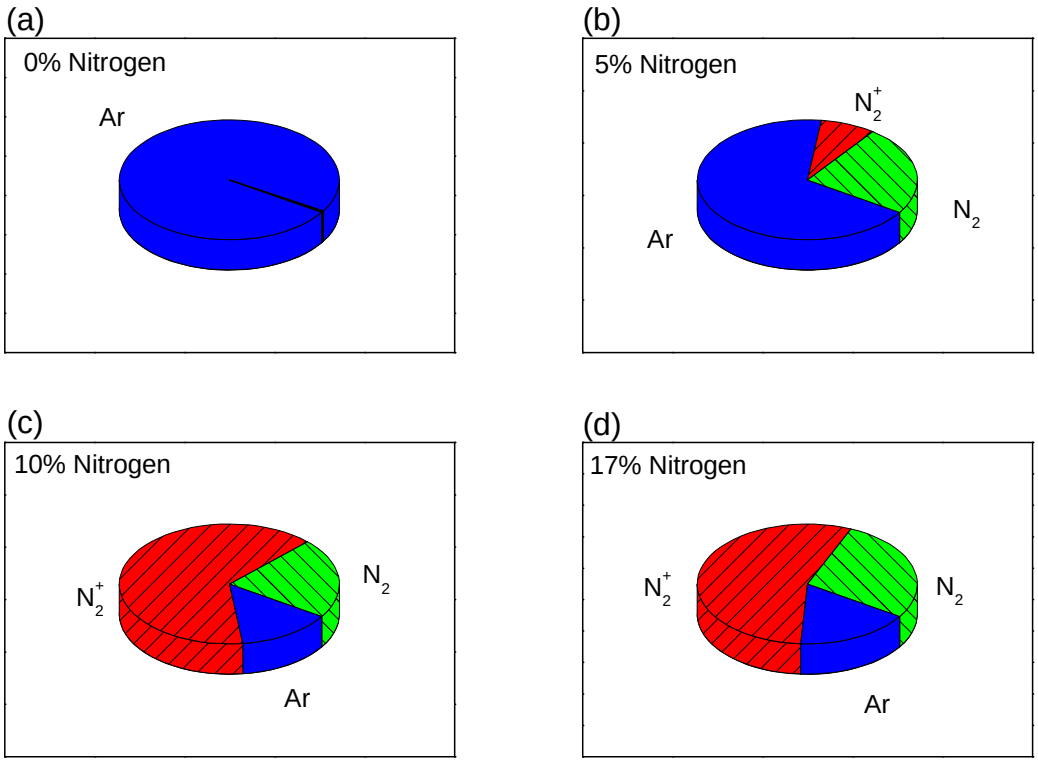

FIG. 5. Pie charts representing relative intensities of emission from argon (blue), molecular nitrogen neutrals (green) and molecular nitrogen ions (red) in the 360 nm − 430 nm range. Specifically, the intensity of the Ar I line at 415.9 nm is compared with the peak intensity of the N_2 SPS bandhead at 380.5 nm ($\Delta\nu$=−2) and the peak intensity of the N_2^+ FNS bandhead at 391.4 nm ($\Delta\nu$=0). The four charts represent (a) no nitrogen seeding, (b) 5% of nitrogen, (c) 10% of nitrogen and (d) 17% of nitrogen. The N_2^+ is the dominating ion for nitrogen seeding fractions of 10% and above. Argon line intensity for cases (c) and (d) is most likely overestimated due to overlap with the N_2^+ FNS band ($\Delta\nu$=−2).

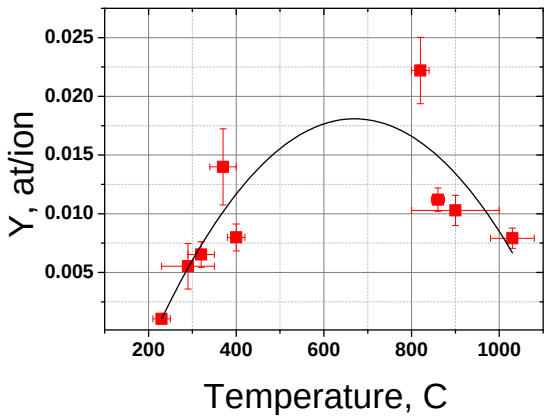

FIG. 6. Chemical sputtering yield of graphite by nitrogen as a function of surface temperature in Pilot-PSI. All samples were electrically floating. The datapoints are fitted empirically with a second order polynomial.

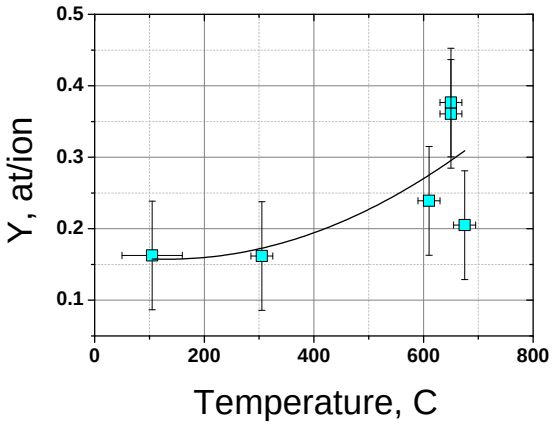

FIG. 7. Chemical sputtering yield of graphite by nitrogen as a function of surface temperature in nano-PSI. Bias voltage was equal to −30 V for all samples. The datapoints are fitted empirically with a second order polynomial.

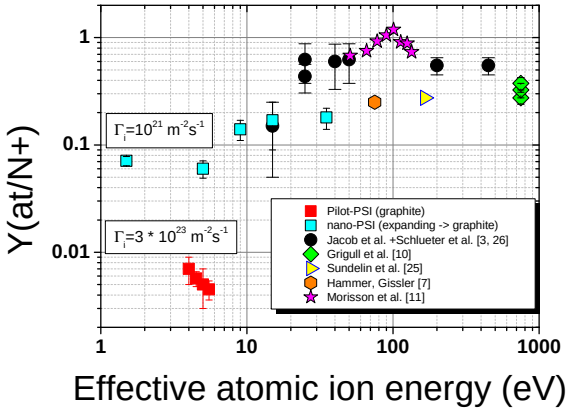

FIG. 8. Sputtering yields of carbon by nitrogen as a function of the effective atomic ion energy. In case of molecular ions interacting with the surface it is assumed that the energy is divided evenly between the two nitrogen atoms. Data from Pilot-PSI and nano-PSI is corrected for differences in surface temperature, using empirical fits from Figures 6 and 7, respectively. Data from other experiments is not corrected.

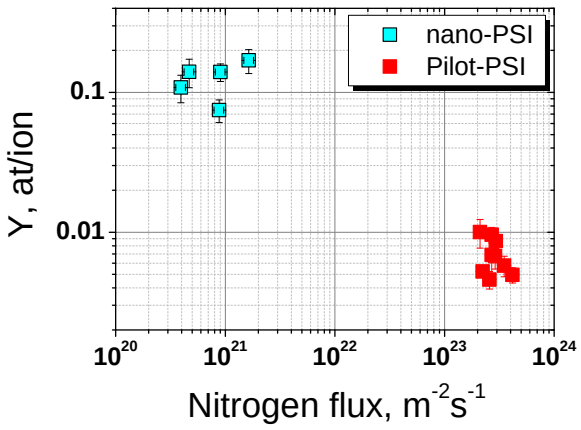

FIG. 9. Chemical sputtering yields of carbon by nitrogen plotted versus the ion flux density. Data from Pilot-PSI and nano-PSI is corrected to account for differences in surface temperature and ion energy.

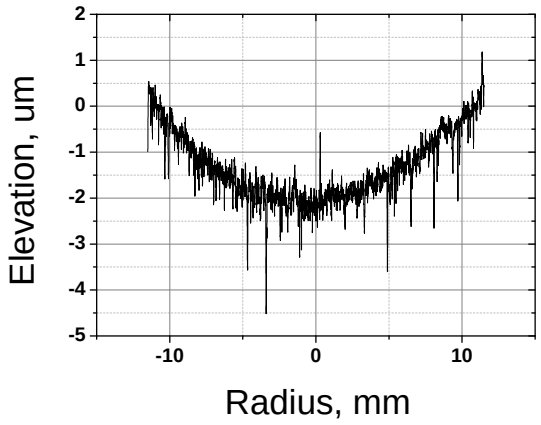

FIG. 10. Results of the surface profilometry measurement for a graphite sample exposed to nitrogen plasma in Pilot-PSI. The edges of the sample, masked from the plasma, are used as a reference level.

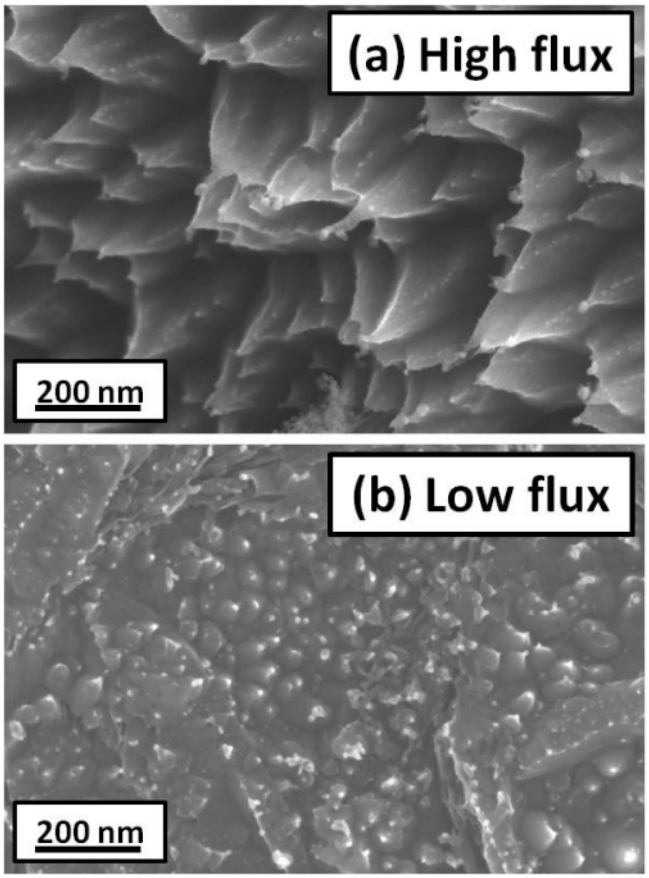

FIG. 11. SEM images of the morphology changes on graphite surfaces exposed to nitrogen plasmas in Pilot-PSI and nano-PSI.